

## STUDY ON CHARACTERISTICS OF FLUID-FLOW AND HEAT TRANSFER IN THE TORSIONAL FLOW HEAT EXCHANGER WITH DROP-SHAPED TUBE

by

**Yongqing WANG, Qianxin ZHANG, Guan WANG,  
Ning LI, Cheng CHEN, and Xin GU\***

School of Mechanical and Power Engineering, Zhengzhou University, Zhengzhou, China

Original scientific paper

<https://doi.org/10.2298/TSCI210712297W>

*Adopting enhanced tube is an effective way to enhance the performance of a shell-and-tube heat exchanger. In this paper, a drop-shaped tube with streamlined cross-section was used to enhance heat transfer of the torsional flow heat exchanger. The characteristics of the fluid-flow and heat transfer in torsional flow heat exchanger with drop-shaped tube were studied numerically, considering three kinds of axis ratios ( $a/b=1.5, 1.8, 2$ ) of the tube. The reliability of numerical results was verified through experimental results. The results indicate that the wake size of the streamlined drop-shaped tube is smaller than that of the conventional smooth tube, and the drop-shaped tube reduces the flow dead zone in torsional flow heat exchanger. As the axis ratio of  $a/b$  increases, the shell side Nusselt number and comprehensive performance increase, due to enhancement of the turbulence kinetic energy of the transition section. When the axis ratio is 2, the Nusselt number is increased by 12.44-18.99%, and the comprehensiveness is increased by 13.27-19.2%, compared with the torsional flow heat exchanger with the smooth tube. The quantitative analysis of the velocity indicates that the relative magnitude and proportion of transverse velocity components of fluid are important factors affecting the thermal-hydraulic performance of torsional flow heat exchanger.*

Key words: shell-and-tube heat exchanger, drop-shaped tube, torsional flow, velocity components

### Introduction

As the world energy situation continues to become severe, improving energy efficiency has become one of the most concerned issues. Shell-and-tube heat exchangers (STHX) are widely used in industrial processes due to their stable performance, and various structures and components have been developed and applied to improve efficiency. According to difference of flow patterns in the shell side, the STHX can be divided into three types: transverse flow, longitudinal flow, and helical flow. The STHX with segmental baffle is a typical representative of transverse flow STHX. With strong heat exchange capacity, it occupies most of the market, but the dead zone on the back of the baffle can lead to scaling and heat transfer deterioration [1]. The rod baffle instead of the segmental baffle effectively eliminates the flow dead zone. The fluid in shell side flows longitudinally in the absence of block from the baffle, and the flow resistance is reduced at the expense of some heat exchange capacity [2]. The helical flow

\* Corresponding author, e-mail: [guxin@zzu.edu.cn](mailto:guxin@zzu.edu.cn)

is considered to be an optimal flow pattern, but the great difficulty of manufacturing continuous spiral baffles limits its wide application in the industry [3]. Although the emergence of various discontinuous helical baffles reduces the difficulty of manufacturing, the weakening of the performance of the shell side by the triangular leakage area is a problem that cannot be ignored [4]. Based on the advantages and disadvantages of different typical flow patterns, Gu *et al.* [5] uses obliquely arranged shutter baffles as a supporting structure to promote the oblique flow of fluid, that is, maintaining the strong scouring effect of the transverse flow on the tube bundle, and inheriting the advantages of small flow resistance of the longitudinal flow. A new STHX with shutter baffle was presented by Lei *et al.* [6] to avoid the abrupt change in the flow direction, and the heat transfer coefficient per pressure drop is 73.3-89.7% higher than that of the STHX with segmental baffle. Gu *et al.* [7] replaced the shutter baffle by the trapezoidal baffle to increase the fluid turbulence intensity. At the same time, two adjacent groups of baffles are arranged orthogonally to strengthen fluid mixing. The results show that fluid-flow pattern in the shell side of STHX with trapezoidal baffle is closer to the ideal oblique flow, and the comprehensive performance is 5.85-9.06% higher than that of STHX with segmental baffle and 15.27-23.28% higher than that of STHX with shutter baffle. The trapezoidal baffle can be cut from the segmental baffle, which also has advantages in manufacturing and installation. Since the fluid-flow pattern in the shell side of the new STHX shows periodic torsion while flowing obliquely, Gu *et al.* [8] named it the torsional flow heat exchanger (TFHX). The previous optimizations of the TFHX focused mainly on the baffle, and the optimization of the heat exchange tube was not involved [8, 9]. Therefore, it is very necessary to evaluate the performance of the TFHX by using the enhanced tube.

Variable cross-section tubes have been extensively studied by scholars, such as corrugated tubes [10], ribbed tubes [11], grooved tubes [12], finned tubes [13], *etc.* These enhanced tubes expand the heat transfer area, and the irregular channels destroy the boundary-layer on the tube side or shell side, so as to enhance the heat transfer at the cost of greater flow resistance. In addition, the complex process is also a key concern [14]. Based on this, the streamlined tubes that can be extruded from smooth tubes have attracted attention. Dogan *et al.* [15] compared the performance of elliptical tube (axial ratio within 0.307-1) and smooth tube in plain fin heat exchangers. The streamline model illustrated that the wake area of the smooth tube is active and has a higher pressure drop, while the wake size of the elliptical tube is smaller and decreases with the decrease of axial ratio. The experimental results of Hasan and Siren [16] showed that the thermal-hydraulic characteristics of staggered elliptical tubes are 1.93-1.96 times of that of smooth tubes. He *et al.* [17] conducted experiments on the air side of the finned tube heat exchanger. They found that the heat transfer coefficient of the elliptical tube was 66% superior to that of the smooth tube. It is revealed that the mechanism of heat transfer enhancement of elliptical tube is that the streamlined shape makes the flow field and temperature field more uniform and thin the boundary layer.

In addition to the basic oval tube, more streamlined tubes were developed. Gharbi *et al.* [18] conducted numerical research on the staggered tube bundles of circular, elliptical, and wing-shaped tubes. The results indicated that the streamlined non-circular tubes have lower pressure drop, and the entropy production of elliptical and wing-shaped tubes is small when the Reynolds number is bigger than 15000. Wang *et al.* [19] modified the circular tube into semi-circle and semi-elliptical streamlined sections to reduce the Karman vortex street effect. After the modification, the wake area of the tube is reduced. The streamline diagram illustrated that taking the semicircle as the upstream surface is more in line with the streamline design, and the thermal-hydraulic results indicated that the slender streamline section is conducive to improv-

ing the comprehensive performance of the heat exchanger. Akbari *et al.* [20] compared the air cross-flow characteristics of a single square, elliptic, and cam-shaped tube through experiments, aiming at the influence of the angle of attack. The results show that the performance of the same tube at different angles of attack is quite different, and the optimality performance occurs in the cam-shaped tube with an angle of attack of  $0^\circ$ , which is 128% larger than the smooth tube. Ibrahim and Gomaa [21] obtained similar conclusions about the angle of attack from the study of elliptical tube bundles in cross-flow. Bayat *et al.* [22] and Lavasani *et al.* [23] conducted cross-flow experiments on staggered and in-line cam-shaped tube bundles. The results showed that the thermal-hydraulic performance of the cam-shaped tube bundle was six times that of the smooth tube bundle. The result indicated that replacing smooth tubes by cam-shaped tubes in the heat exchanger can reduce the size of the heat exchanger. Another experiment of Abolfathi *et al.* [24] shows that the cam-shaped tube has better performance in mixed tube bundles. Lavasani *et al.* [25] and Mobedi *et al.* [26] has conducted a detailed study on the blockage ratios and aspect ratios of the cam-shaped tube, and the conclusion is that increasing the blockage ratio and aspect ratio can reduce the drag coefficient. The streamlined tube developed by Park *et al.* [27] is similar to the cam-shaped and has excellent results. He *et al.* [28] applied the elliptical tube to the STHX with helical baffle, which increased the Nusselt number on the shell side by 11.4-16.6% and reduced the friction coefficient by 29.2-36.9%. Du *et al.* [29] optimized the layout of the elliptical tubes in the STHX with helical baffle to adapt to the helical flow pattern, and the optimized overall performance was increased by 50%. The conclusions indicate clearly that the streamlined tube has satisfied performance at the right angle of attack.

In summary, the streamlined tube has a significant improvement in the flow field, and presents advantages in heat transfer enhancement. It is appropriate to use streamlined tubes in STHX, but the development of streamlined tubes also needs to be based on the complex flow patterns in STHX. To extend the application of streamlined tubes in STHX, in this paper, a drop-shaped tube with a streamlined cross-section is adopted in TFHX to strengthen its performance. Furthermore, the cross-section is periodically twisted to achieve the optimized angle of attack. The fluid-flow and heat transfer characteristics in torsional flow heat exchanger with drop-shaped tube (TFHX-DT) were investigated numerically, and which is compared with the torsional flow heat exchanger with smooth tube (TFHX-ST). The idea of matching the tube shape with the flow pattern can provide a reference for the development of advanced STHX.

## Numerical modelling

### *Geometrical model*

The cross-section of drop-shaped tube is a water drop shape, which is composed of semi-circle and semi-ellipse. The main geometric parameters include the semi-major axis  $a$  of ellipse and the radius  $b$  of circle. Here, the perimeter of drop-shaped tube is constant same as the perimeter of the smooth tube with outer diameter of 19 mm. The two straight sections,  $L_s$ , of the drop-shaped tube are connected by a smoothly twisted  $90^\circ$  transition section,  $L_t$ , to realize the alternate twist of the cross-section. The overall model of TFHX-DT with  $a/b$  ratios of 1.5, 1.8, 2 are established respectively [15, 26], as illustrated in fig. 1. In the overall model of TFHX-DT, a group of trapezoid inclined baffles is installed on a straight section, and the drop-shaped tube transition section is set between the two groups of baffles. The orthogonally arranged baffles match the twisting direction of drop-shaped tube to ensure the angle of fluid impacting the tube bundles at different baffles is consistent. Detailed dimensions are listed in tab. 1.

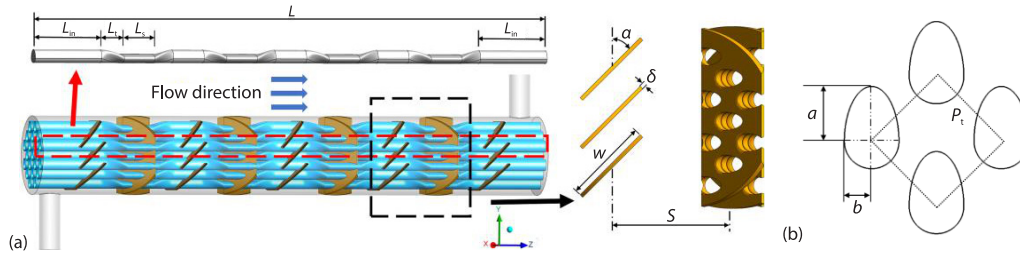


Figure 1. Sketches of TFHX-DT; (a) models of TFHX-DT and (b) cross-section and layout

Table 1. Main parameters of TFHX

Parameters	Size	Parameters	Size
Shell inner diameter [mm]	150	Baffles spacing, $S$ [mm]	100
Number of tubes, $N$ [-]	21	Angle of baffle, $\alpha$ [ $^\circ$ ]	45
Length, $L$ [mm]	1000	Baffle width, $w$ [mm]	70
Tube pitch, $P_t$ [mm]	25	Baffle thickness, $\delta$ [mm]	3
$L_{in}$ , $L_{out}$ [mm]	130	Diameter of inlet and outlet [mm]	40
Straight section, $L_s$ [mm]	60	Axis ratios, $a/b$ [-]	1.5, 1.8, 2
Transition section, $L_t$ [mm]	40	Layout	Rotated square

### Governing equation and boundary conditions

Continuity equation:

$$\frac{\partial}{\partial x_i}(\rho u_i) = 0 \quad (1)$$

Momentum equation:

$$\frac{\partial}{\partial x_j}(\rho u_j u_i) = -\frac{\partial p}{\partial x_i} + \mu \frac{\partial}{\partial x_j} \left( \frac{\partial u_i}{\partial x_j} \right) \quad (2)$$

Energy equation:

$$\frac{\partial}{\partial x_j}(\mu_j T) = \frac{\lambda}{\rho c_p} \frac{\partial}{\partial x_j} \left( \frac{\partial T}{\partial x_j} \right) + \frac{S_T}{\rho} \quad (3)$$

The shell side fluid is in a turbulent state with a strong secondary flow and swirling flow. The RNG  $k$ - $\varepsilon$  model was used to process high strain rate and streamline curvature in the shell side [4]:

$$\frac{\partial}{\partial x_i}(\rho k u_i) = \frac{\partial}{\partial x_j} \left( \alpha_k \mu_{\text{eff}} \frac{\partial k}{\partial x_j} \right) + G_k + \rho \varepsilon \quad (4)$$

$$\frac{\partial}{\partial x_i}(\rho \varepsilon u_i) = \frac{\partial}{\partial x_j} \left( \alpha_\varepsilon \mu_{\text{eff}} \frac{\partial \varepsilon}{\partial x_j} \right) + C_{1\varepsilon} \frac{\varepsilon}{k} G_k - C_{2\varepsilon} \rho \frac{\varepsilon^2}{k} - \frac{\varepsilon \eta G_k \left( 1 - \frac{\eta}{\eta_0} \right)}{k(1 + \beta u^3)} \quad (5)$$

where

$$\mu_{\text{eff}} = \mu + \mu_t, \quad \mu_t = \frac{\rho C_\mu k^2}{\varepsilon}, \quad G_k = 2\mu_t S_{ij} S_{ij}, \quad \eta = \left(2S_{ij} S_{ij}\right)^{1/2} \frac{k}{\varepsilon}, \quad S_{ij} = \frac{1}{2} \left( \frac{\partial u_i}{\partial x_j} + \frac{\partial \mu_j}{\partial x_i} \right)$$

$$C_\mu = 0.0845, \quad C_{1\varepsilon} = 1.42, \quad C_{2\varepsilon} = 1.68, \quad \alpha_k = \alpha_\varepsilon = 1.39, \quad \eta_0 = 4.38, \quad \beta = 0.012$$

Incompressible water was used as the working fluid, and the calculation process was not due to gravity. The inlet was velocity-inlet, while the inlet temperature was 293.15 K. The outlet was pressure-outlet with 0 Pa. The wall temperature was constant at 393.15 K, and the shell wall and support structure were non-slip adiabatic conditions. The standard wall function method was used to deal with the near wall region. The pressure-velocity coupling adopted the SIMPLE algorithm, and the second-order upwind scheme was applied to solve momentum and energy equations.

#### Grid generation and data reduction

The *poly-hexcore* hybrid grid was used to mesh the computational domain. The details of grids are shown in fig. 2. In order to obtain reliable simulation results, the grid independence was tested under the mass flow rate of 1.71 kg/s. The variation of numerical results with the number of grids is shown in fig. 3. When the grid numbers are 2482250, the relative error is less than 1.5%, with which the calculation is considered as a grid-independent solution.

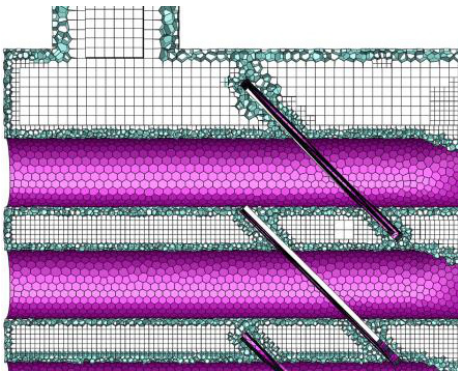


Figure 2. Grids details

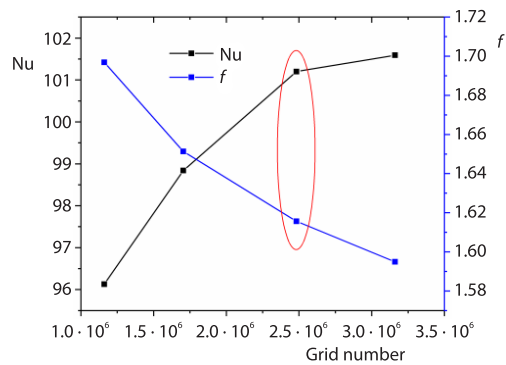


Figure 3. Independence test

The equation of data processing is defined. The heat transfer coefficient is as follows

[4]:

$$h = \frac{\dot{m} c_p (t_{\text{out}} - t_{\text{in}})}{A \Delta t_m} \quad (6)$$

$$A = N C_d L \quad (7)$$

$$C_d = \frac{\pi}{2} \left[ \frac{3}{2} (a + b) - (ab)^{1/2} + 2b \right] \quad (8)$$

$$\Delta t_m = \frac{(t_w - t_{\text{in}}) - (t_w - t_{\text{out}})}{\ln \frac{t_w - t_{\text{in}}}{t_w - t_{\text{out}}}} \quad (9)$$

Nusselt number and friction factor [10]:

$$\text{Nu} = \frac{hd_e}{\lambda} \quad (10)$$

$$f = \frac{2\Delta p d_e}{\rho U^2 L} \quad (11)$$

where  $d_e$  is the equivalent diameter. For the TFHX-DT with rotated square tube arrangement [28]:

$$d_e = \frac{4 \left[ P_t^2 - \frac{\pi}{2} (ab + b^2) \right]}{\frac{\pi}{2} \left[ \frac{3}{2} (a + b) - (ab)^{1/2} + 2b \right]} \quad (12)$$

Performance evaluation criterion (PEC) is used as an index of comprehensive performance [10]:

$$\text{PEC} = \frac{\text{Nu}}{\text{Nu}_0} \left( \frac{f}{f_0} \right)^{1/3} \quad (13)$$

where  $\text{Nu}_0$  and  $f_0$  are the corresponding values of the smooth tube. The value of PEC exceeds 1 means that the performance of the TFHX-DT is superior to that of the TFHX-ST.

## Verification of numerical simulation

### Experimental procedures

An experimental model of TFHX was made to verify the numerical calculations, and the experimental laser doppler velocimeter (LDV) system was built to test the velocity in the model. The experimental model with rectangular cross-section was made of plexiglass to reduce the refraction of the laser beams. Model details are presented in fig. 4. To eliminate interference from the tube outer wall to the laser, the measurement points were set on two straight lines paralleling the Z-axis between the tubes. The positions of two measurement lines are shown in fig. 5.

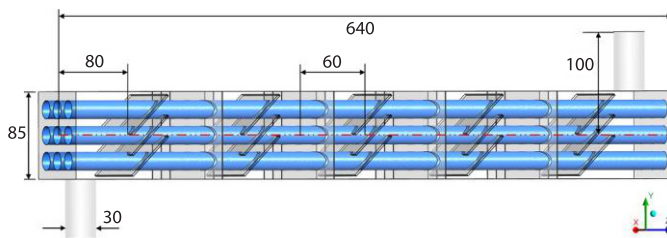


Figure 4. Experimental model

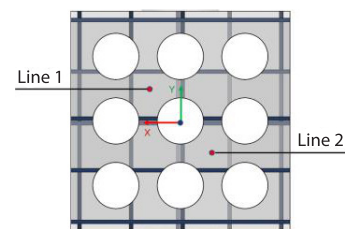
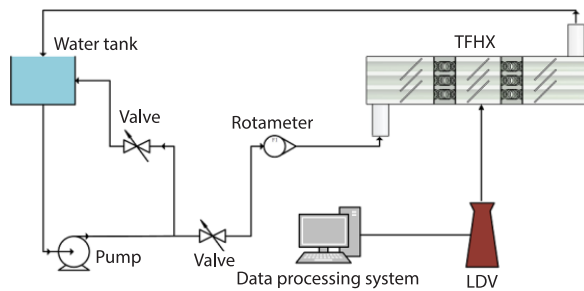


Figure 5. Locations of measured line

In the experiment, hollow glass tracer TSI10089 was added as the tracer into the water. The fluid with tracer particles passes through the pump, rotameter, heat exchanger model, and water tank in turn. The velocity of the tracer particles was measured by the LDV, and the data were obtained and processed by the software FLOWSIZER. The specific types of the main devices are presented in tab. 2, and the sketch of experimental procedures is illustrated in figs. 6 and 7. With all the mentioned errors, the experimental uncertainty is 2.63% [28].

**Table 2. Parameters of the experimental devices**

Name	Type or parameter	Name	Type or parameter
LDV		Booster pump	
Fiber-optical probe	TR×60	Type	MJ-NS 6500
Laser out-put power [W]	2	Power [W]	85
Lens	TLN06-350	Maximum flow [Lh <sup>-1</sup> ]	3800
Lens focal length [mm]	363	Maximum head [m]	3.5
Laser wavelengths [nm]	488, 514.5	Rotameter	
Standard beam diameter [mm]	2.65	Type	LZB-50
Fringe spacing [μm]	3.7	Measurement range [m <sup>3</sup> h <sup>-1</sup> ]	0.6-6
Measurement/installation accuracy	±0.2%-0.8%	Measurement accuracy	±2.5%



**Figure 6. Sketch of the experiment procedures**

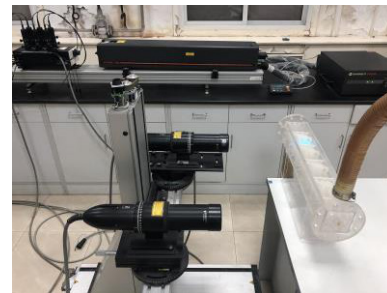


**Figure 7. Laser devices**

### Experimental results

The velocity values of fluid on Line 1 and Line 2 were obtained numerically with the volume flow rate of 4 m<sup>3</sup>/h, and which are compared with the experimental values. The details are illustrated in figs. 8 and 9. The experiment values are in good agreement with the numerical solutions, and the average errors on Line 1 and Line 2 are 13.77% and 14.23%, separately, thus the accuracy of the numerical simulation method is verified.

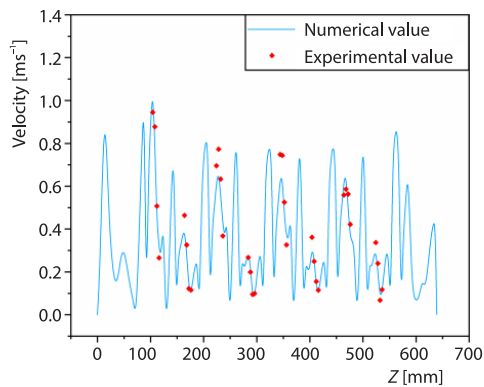


**Figure 8. Fluid velocity comparison on Line 1**

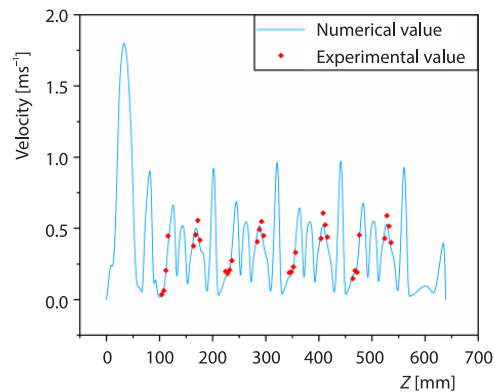


**Figure 9. Fluid velocity comparison on Line 2**

## Results and discussion

### Effect of drop-shaped tube

According to the common working conditions of the shell side of STHX, the five mass flow rates of 1.14 kg/s, 1.71 kg/s, 2.28 kg/s, 2.85 kg/s, 3.71 kg/s, and 5.98 kg/s were selected to carry out in the present work. These five mass flow rates correspond to the Reynolds numbers of 4000, 6000, 8000, 10000, 13000, and 21000 in the shell side of TFHX-ST, which are typical turbulent states. The calculation of Reynolds number same as that in [7].

Figure 10 shows the velocity distribution of TFHX-ST and TFHX-DT with  $a/b$  of 1.8 at a group of baffles while the mass-flow rate is 3.71 kg/s. The section position is on the plane of  $X = 0$ . Section A is located between two groups of baffles and is also a straight section of drop-shaped tube. In this section, the drop-shaped tube is more streamlined than the smooth tube for the incoming flow, and also has a certain diversion effect. Therefore, the degree of fluid scouring on the wall of TFHX-DT is more intense. In Sections B and C, it is found that TFHX-ST has obvious flow dead zones, which is due to that the fluid between the baffles and near the cylinder is blocked by the downstream baffles and which leads to some fluid to back-flow [8]. In TFHX-DT, the flow dead zone areas of these two regions are obviously reduced. Section B is located in the straight section of drop-shaped tube. The diversion effect of drop-shaped tube makes part of high-speed fluid close to the cylinder flow obliquely upward, which weakens the backflow and enhances the scouring on the tube wall. Section C is located in the transition section, where the twisted tube enhances the disturbance in this region and increases the fluid velocity.

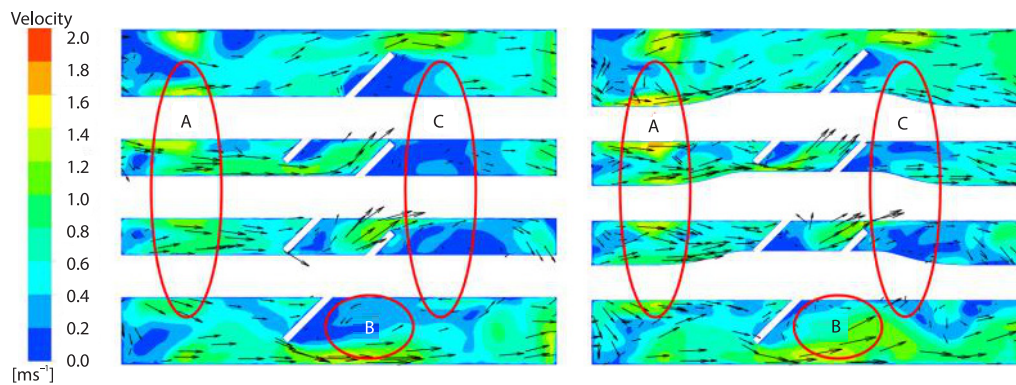
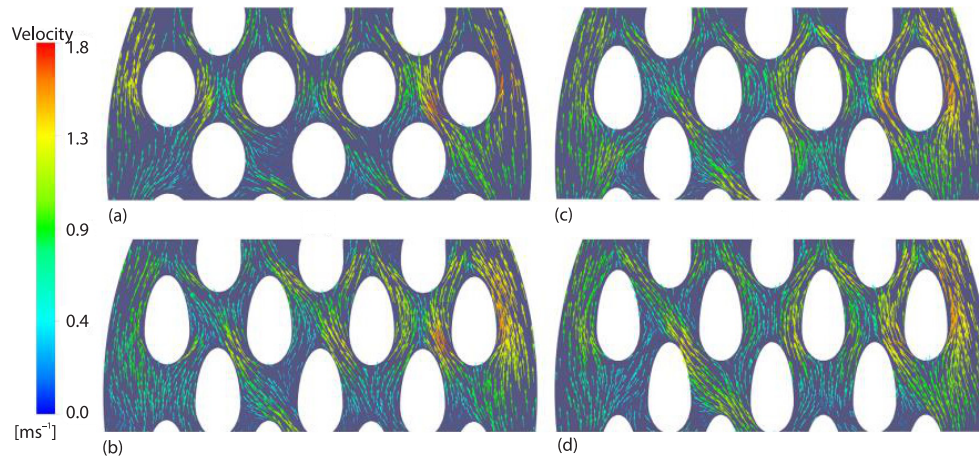


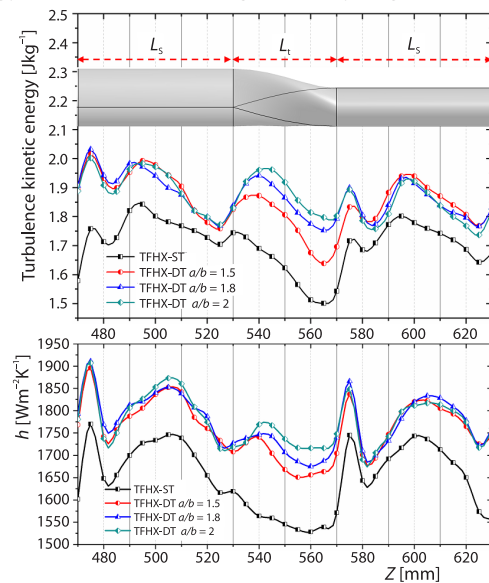
Figure 10. Velocity distribution in shell sides of TFHX-ST and TFHX-DT with  $a/b$  of 1.8

Figure 11 illustrates the tangential velocity vector at the surface of an inclined baffle to observe clearly the effect of the streamlined section on oblique flow. The fluid-flowing from the upstream gap hits the downstream tube wall and is redistributed. The turbulent intensity of the distributed fluid increases and scours the tube bundle obliquely. For the smooth tube, the streamlined section of drop-shaped tube more fits the incoming flow and strengthens the diversion effect of the inclined baffle. The distributed fluid is close to the wall of drop-shaped tube, especially on its back, and the flow condition in the wake section is improved. The size of wake area decreases with the increase of  $a/b$ , and the flow between tube bundles is smoother, which is conducive to the reduction of flow resistance.



**Figure 11. Tangential velocity vector at inclined baffle; (a) TFHX-ST, (b) TFHX-DT  $a/b = 1.5$ , (c) TFHX-DT  $a/b = 1.8$ , and (d) TFHX-DT  $a/b = 2$**

There is no doubt that the drop-shaped tube has a positive effect on the flow of TFHX, which will also lead to varieties in heat transfer performance. Heat transfer performance is closely related to turbulent flow. Figure 12 shows the variation of turbulence kinetic energy and local heat transfer coefficient along the direction of Z-axis [10]. The selected interval is in the fully developed region of flow, including two straight sections and the transition section between them. It is seen that the local heat transfer coefficient and turbulence energy have similar change trend. The turbulence kinetic energy of TFHX-DT is significantly higher than that of TFHX-ST due to the improvement of flow by the drop-shaped tube. Correspondingly, the local heat transfer coefficient of TFHX-DT is 2.39-13.37% higher than that of TFHX-ST. In other words, the high turbulence kinetic energy brought by the drop-shaped tube to the shell side fluid of TFHX makes the thermal performance of TFHX-DT better than that of TFHX-ST. In the straight section, the influence of  $a/b$  on the turbulence kinetic energy of TFHX-DT has no significant regularity, because the dominance of the baffle weakens the impact brought about by the change of  $a/b$ . In the transition section without baffles, the turbulence kinetic energy is positively correlated with  $a/b$ . The increase of  $a/b$  means a more serious degree of distortion, which will bring strong turbulent flow. The difference of turbulence state in the transition section is the direct cause of that the thermal performance increases with the increase of  $a/b$ .



**Figure 12. Turbulent kinetic energy and local  $h$  vs.  $Z$**

It is also interesting that the trend of turbulence kinetic energy in the two straight sections is very similar, despite their different directions, and there is a similar performance in terms of local heat transfer coefficient. Obviously, the periodic arrangement of the baffle and

the periodic twisting of the drop-shaped tube makes that the characteristic values are similar in the directions of  $X$ -axis and  $Y$ -axis.

#### *Thermal-hydraulic performance in shell side*

Figures 13 and 14 demonstrate the change trends of Nusselt number and friction factor with mass-flow rate. The multiple improvements of the streamlined tube to the flow field make that the Nusselt number of TFHX-DT is superior to TFHX-ST, and the high turbulence kinetic energy caused by the increase of  $a/b$  increases the Nusselt number of the shell side. The Nusselt number of TFHX-DT with  $a/b = 2$  is enhanced by 12.44-18.99% than that of TFHX-ST. From fig. 14, the drop-shaped tube improves the thermal performance of the shell side, while also reduces its friction factor.

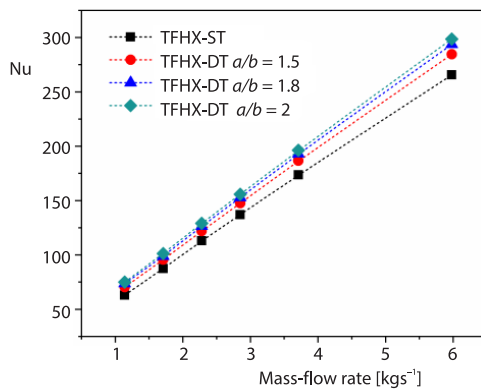


Figure 13. The Nu versus mass-flow rate

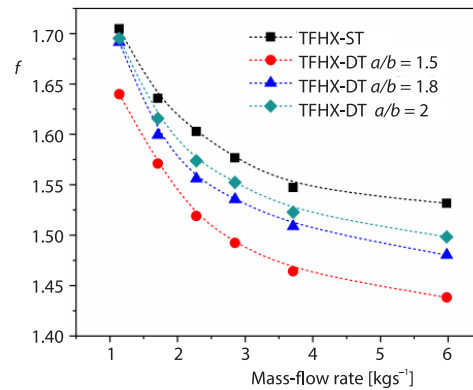


Figure 14. Friction factor vs. mass-flow rate

The friction factor of TFHX-DT with  $a/b$  of 1.5 is the smallest, which is 3.8-6.09% lower than that of TFHX-ST. The streamlined structure of drop-shaped tube increases the velocity of the shell side, while reduces the flow resistance. These trends convey that the enhancement of the thermal performance of TFHX-DT by the drop-shaped tube is not at the expense of extra energy consumption.

The trends of the PEC of TFHX-DT based TFHX-ST are illustrated in fig. 15. The comprehensive performance is improved markedly when the smooth tube is replaced by the

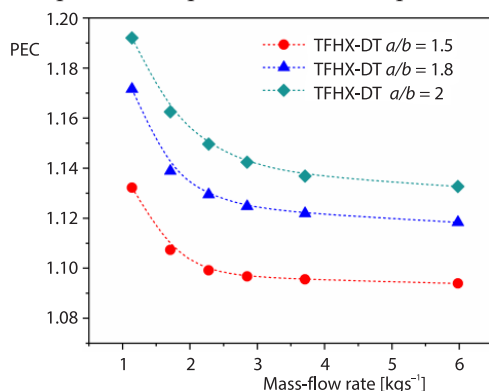


Figure 15. The PEC of TFHX-DT

drop-shaped tube with the same cross-section perimeter. Within studied mass-flow range, the comprehensive performance of TFHX-DT with  $a/b$  of 1.5, 1.8, and 2 is improved by 9.39-13.22%, 11.83-17.16%, and 13.27-19.2% by compared with that of TFHX-ST, separately. Numerical results indicate that the combination of drop-shaped tube and TFHX heighten effectively the thermal efficiency, which is the product of matching the special flow pattern of TFHX with the shape of the tube. With the same perimeter, the improvement of the streamlined degree of drop-shaped tube improves the comprehensive performance of TFHX-DT.

*Flow velocity in shell side*

Fluid-flow patterns in STHX can be summarized as fluid-flowing through the tube bundles. Different from the ideal crossflow tube bundles, the fluid scouring the tube bundles are under the diversion effect of various baffles and tubes, which is one of the main reasons for the difference of performance of shell side [30]. The difference in the state of cross-flow caused by baffles and tubes is reflected by the changes in flow velocity along the *X*-, *Y*-, and *Z*-axes. The transverse velocity component perpendicular to the tube bundle is defined as  $U_c$ , and the longitudinal velocity component parallel to the tube bundle is defined as  $U_\ell$ , which can be calculated by eqs. (14) and (15) [30].

$$U_c = \frac{1}{V} \int U_c dV = \frac{1}{V} \sum_{i=1}^n (u_i^2 + v_i^2)^{1/2} |V_i| \tag{14}$$

$$U_\ell = \frac{1}{V} \int U_\ell dV = \frac{1}{V} \sum_{i=1}^n w_i |V_i| \tag{15}$$

where,  $u$ ,  $v$ ,  $w$  are the velocity along *X*-, *Y*-, and *Z*-axes and  $V$  is the total volume of the shell side.

A user-defined function (UDF) program was used to calculate the velocity component of fluid in TFHX-DT, and their ratio reflects the relationship between them. Detailed data are presented in tab. 3. The data show that the transverse velocity component of TFHX-DT is greater than that of TFHX-ST at the same mass-flow rate. The maximum discrepancy between TFHX-ST and TFHX-DT with  $a/b$  of 1.5 is 6.59%, and the minimum discrepancy is 5.87%. This gap does not change obviously with the change of mass-flow rate, and there are similar conclusions for TFHX-DT with values of  $a/b$  of 1.8 and 2. The difference between the longitudinal velocity components of TFHX-ST and TFHX-DT is not obvious, and the maximum is only 2.64%. The overall velocity statistics indicates that the main influence of drop-shaped tube increases the transverse velocity component, and the degree of influence depends on the structure of drop-shaped tube and does not vary with the mass-flow.

**Table 3. Velocity components on the shell side**

$\dot{m}$ [kgs <sup>-1</sup> ]		1.14	1.71	2.28	2.85	3.71	5.98	Average
TFHX-ST	$U_c$	0.1243	0.1887	0.2554	0.3208	0.4203	0.6831	–
	$U_\ell$	0.1117	0.1692	0.2278	0.2851	0.3743	0.6054	–
	$U_c/U_\ell$	1.113	1.115	1.121	1.125	1.123	1.128	1.121
TFHX-DT $a/b = 1.5$	$U_c$	0.1316	0.2005	0.2713	0.3408	0.4480	0.7269	–
	$U_\ell$	0.1137	0.1726	0.2326	0.2907	0.3824	0.6214	–
	$U_c/U_\ell$	1.157	1.162	1.166	1.172	1.172	1.170	1.167
TFHX-DT $a/b = 1.8$	$U_c$	0.1309	0.1999	0.2708	0.3406	0.4459	0.7232	–
	$U_\ell$	0.1117	0.1707	0.2305	0.2889	0.3765	0.6092	–
	$U_c/U_\ell$	1.172	1.171	1.175	1.179	1.184	1.187	1.178
TFHX-DT $a/b = 2$	$U_c$	0.1303	0.2003	0.2694	0.3383	0.4445	0.7228	–
	$U_\ell$	0.1110	0.1691	0.2276	0.2845	0.3748	0.6065	–
	$U_c/U_\ell$	1.174	1.185	1.184	1.189	1.186	1.192	1.185

For TFHX-DT, due to the increase of  $a/b$  makes the drop-shaped tube flatter, the flow area between the tube bundles increases, so the average velocity of the shell side decreases slightly. However, the average ratio of velocity component rises with the increase of  $a/b$ , in other words, the proportion of transverse flow scouring the tube bundle rises with the increase of  $a/b$ . Combining the trend of positive correlation between the Nusselt number and  $a/b$ , it is concluded that the relative magnitude of the transverse velocity component is a considerable factor that affects the thermal performance of TFHX-DT, meanwhile, the rise of the proportion of transverse velocity component would also improve its thermal performance.

### Conclusions

In this investigation, the streamlined drop-shaped tube is used to strengthen the performance of TFHX, and the characteristics in TFHX-DT are numerically studied in the turbulent flow conditions of 1.14-5.98 kg/s. The influences of axis ratio ( $a/b = 1.5, 1.8, 2$ ) on thermal-hydraulic performance were discussed. The conclusions are as follows.

- The LDV speed measurement experiment was carried out, and the average error between the experimental result and the numerical result was 13.77% and 14.23%. The acceptable error confirmed that the numerical result was reliable.
- The size of the wake area of the streamlined drop-shaped tube is smaller than that of the smooth tube, which makes the shell side flow field smoother. The minimum value of the friction factor goes to the TFHX-DT with  $a/b = 1.5$ , which is lower 3.8-6.09% than that of TFHX-ST. The existence of the transition section increases the disturbance and reduces the flow dead zone.
- The high turbulence kinetic energy brought by the drop-shaped tube to the shell side fluid of TFHX makes the thermal performance of TFHX-DT better than that of TFHX-ST. The reason for the positive correlation between thermal performance and  $a/b$  is the difference in turbulence kinetic energy in the transition section. Increasing the streamlined degree of drop-shaped tube can improve the comprehensive performance of TFHX-DT. The TFHX-DT with  $a/b$  of 2 has the highest comprehensive performance, which is higher 13.27-19.2% than that of TFHX-ST.
- The overall velocity statistics show that the influence of drop-shaped tube on TFHX can be reflected in the increase of the transverse velocity component. The thermal-hydraulic performance of TFHX-DT is not only related to the relative magnitude of the transverse velocity component but also affected by its proportion.

### Acknowledgement

This work is supported by National Natural Science Foundation of China (Grant No. 21776263 and No. 51776190).

### Nomenclature

$a$ – ellipse semi-major axis, [mm]	$L_t$ – length of transition section, [mm]
$A$ – heat exchange surface area, [m <sup>2</sup> ]	$\dot{m}$ – mass-flow rate, [kg s <sup>-1</sup> ]
$b$ – circle radius, [mm]	$N$ – number of tubes, [–]
$C_d$ – perimeter, [mm]	$Nu$ – Nusselt number ( $=hd_c/\lambda$ ), [–]
$c_p$ – specific heat capacity, [J kg <sup>-1</sup> K <sup>-1</sup> ]	$P_t$ – tube pitch, [mm]
$d_e$ – equivalent diameter, [mm]	$\Delta p$ – pressure drop, [Pa]
$f$ – friction factor ( $=2\Delta pd_c/\rho U^2 L$ ), [–]	$S$ – baffles spacing, [mm]
$h$ – heat transfer coefficient, [W m <sup>-2</sup> K <sup>-1</sup> ]	$t$ – fluid temperature, [K]
$L$ – length of tube, [mm]	$\Delta t_m$ – log-mean temperature difference, [K]
$L_s$ – length of straight section, [mm]	$U$ – fluid velocity, [m s <sup>-1</sup> ]

$U_c$  – transverse velocity component, [ms<sup>-1</sup>]  
 $U_l$  – longitudinal velocity component, [ms<sup>-1</sup>]  
 $V$  – total volume of the shell side, [m<sup>3</sup>]  
 $w$  – baffle width, [mm]

#### Greek symbols

$\alpha$  – angle of baffle, [°]  
 $\delta$  – baffle thickness, [mm]  
 $\lambda$  – fluid thermal conductivity, [Wm<sup>-1</sup>K<sup>-1</sup>]  
 $\rho$  – fluid density, [kgm<sup>-3</sup>]

#### Subscripts

in – inlet  
out – outlet  
w – tube wall

#### Acronyms

LDV – laser doppler velocimeter  
PEC – performance evaluation criterion  
STHX – shell-and-tube heat exchangers  
TFHX – torsional flow heat exchanger  
UDF – user-defined function

#### References

- [1] Zeyninejad Movassag, S., *et al.*, Tube Bundle Replacement for Segmental and Helical Shell and Tube Heat Exchangers: Performance Comparison and Fouling Investigation on the Shell Side, *Applied Thermal Engineering*, 51 (2013), 1-2, pp. 1162-1169
- [2] Dong, Q. W., *et al.*, Numerical and Experimental Investigation of Shellside Characteristics for ROD Baffle Heat Exchanger, *Applied Thermal Engineering*, 28 (2008), 7, pp. 651-660
- [3] Peng, B., *et al.*, An Experimental Study of Shell-and-Tube Heat Exchangers With Continuous Helical Baffles, *Journal of Heat Transfer*, 129 (2007), 10, pp. 1425-1431
- [4] Jian, W., *et al.*, Numerical Investigation on Baffle Configuration Improvement of the Heat Exchanger with Helical Baffles, *Energy Conversion and Management*, 89 (2015), Jan., pp. 438-448
- [5] Gu, X., *et al.*, Contrast Experimental Research on Heat Transfer and Flow Resistance Performance for Tree Kinds of Shell-and-Tube Heat Exchangers, *China Mechanical Engineering*, 23 (2011), 13, pp. 1611-1615
- [6] Lei, Y., *et al.*, Design and Performance Analysis of the Novel Shell-and-Tube Heat Exchangers with Louver Baffles, *Applied Thermal Engineering*, 125 (2017), Oct., pp. 870-879
- [7] Gu, X., *et al.*, Characteristics of Fluid Flow and Heat Transfer in the Shell Side of the Trapezoidal-Like Tilted Baffles Heat Exchanger, *Journal of Thermal Science*, 27 (2018), 6, pp. 602-610
- [8] Gu, X., *et al.*, Analysis of Flow Dead Zone in Shell Side of a Heat Exchanger with Torsional Flow in Shell Side, *Applied Thermal Engineering*, 180 (2020), Nov., 115792
- [9] Gu, X., *et al.*, Multi-Objective Optimization on Structural Parameters of Torsional Flow Heat Exchanger, *Applied Thermal Engineering*, 161 (2019), Oct., 113831
- [10] Wang, W., *et al.*, Numerical Investigation of Tube-Side Fully Developed Turbulent Flow and Heat Transfer in Outward Corrugated Tubes, *International Journal of Heat and Mass Transfer*, 116 (2018), Jan., pp. 115-126
- [11] Gradziel, S., *et al.*, Experimental Determination of the Heat Transfer Coefficient in Internally Rifled Tubes, *Thermal Science*, 23 (2019), Suppl. 4, pp. S1163-S1174
- [12] Selvaraj, P., *et al.*, Computational Fluid Dynamics Analysis on Heat Transfer and Friction Factor Characteristics of a Turbulent Flow for Internally Grooved Tubes, *Thermal Science*, 17 (2013), 4, pp. 1125-1137
- [13] Pongsoi, P., *et al.*, Heat Transfer and Flow Characteristics of Spiral Fin-and-Tube Heat Exchangers: A Review, *International Journal of Heat and Mass Transfer*, 79 (2014), Dec., pp. 417-431
- [14] Yagita, T., *et al.*, Formability Improvement by Die-bearing Grooves in Tube Extrusion with Spiral Inner Projections, *Procedia Engineering*, 81 (2014), Dec., pp. 641-646
- [15] Dogan, S., *et al.*, Numerical Comparison of Thermal and Hydraulic Performances for Heat Exchangers Having Circular and Elliptic Cross-Section, *International Journal of Heat and Mass Transfer*, 145 (2019), Dec., 118731
- [16] Hasan, A., K. Siren, Performance Investigation of Plain Circular and Oval Tube Evaporatively Cooled Heat Exchangers, *Applied Thermal Engineering*, 24 (2004), 5-6, pp. 777-790
- [17] He, S., *et al.*, Heat and Mass Transfer Performance of Wet Air Flowing Around Circular and Elliptic Tube in Plate Fin Heat Exchangers for Air Cooling, *Heat and Mass Transfer*, 55 (2019) 12, pp. 3661-3673
- [18] Gharbi, N. E., *et al.*, Numerical Optimization of Heat Exchangers with Circular and Non-Circular Shapes, *Case Studies in Thermal Engineering*, 6 (2015), Sept., pp. 194-203
- [19] Wang, Q., *et al.*, Analysis on Thermal Hydraulic Performance of the Elliptical Tube in the Finned-Tube Heat Exchanger by New Method, *International Journal of Heat and Mass Transfer*, 134 (2019), May, pp. 388-397
- [20] Akbari, M., *et al.*, Experimental Investigation of the Heat Transfer for Non-Circular Tubes in a Turbulent Air Cross Flow, *Experimental Heat Transfer*, 34 (2021), 6, pp. 513-530

- [21] Ibrahim, T. A., Gomaa, A., Thermal Performance Criteria of Elliptic Tube Bundle in Crossflow, *International Journal of Thermal Sciences*, 48 (2009), 11, pp. 2148-2158
- [22] Bayat, H., *et al.*, Experimental Study of Thermal-Hydraulic Performance of Cam-Shaped Tube Bundle with Staggered Arrangement, *Energy Conversion and Management*, 85 (2014), Sept., pp. 470-476
- [23] Mirabdollah Lavasani, A., *et al.*, Experimental Study of Convective Heat Transfer from in-Line Cam Shaped Tube Bank in Crossflow, *Applied Thermal Engineering*, 65 (2014), 1-2, pp. 85-93
- [24] Abolfathi, S., *et al.*, Experimental Study on Flow Around a Tube in Mixed Tube Bundles Comprising Cam-Shaped and Circular Cylinders in in-Line Arrangement, *International Journal of Thermal Sciences*, 163 (2021), May, 106812
- [25] Lavasani, A. M., *et al.*, Effect of Blockage Ratio on Pressure Drag and Heat Transfer of a Cam-Shaped Tube, *Heat and Mass Transfer*, 52 (2015), 9, pp. 1935-1942
- [26] Mobedi, P., *et al.*, The Aspect Ratio Effect on the Performance of a Cam-Shaped Cylinder in Crossflow of Air, *Experimental Heat Transfer*, 35 (2021), 4, pp. 500-515
- [27] Park, H.-C., *et al.*, Numerical Study for Heat Transfer Characteristics Varying Cross-Sectional Shape of a Tube, *Korean Journal of Air-Conditioning and Refrigeration Engineering*, 24 (2012), 7, pp. 560-566
- [28] He, Z., *et al.*, Numerical Investigation on Performance Comparison of Non-Newtonian Fluid Flow in Vertical Heat Exchangers Combined Helical Baffle with Elliptic and Circular Tubes, *Applied Thermal Engineering*, 100 (2016), May, pp. 84-97
- [29] Du, T., *et al.*, Performance of Continuous Helical Baffled Heat Exchanger with Varying Elliptical Tube Layouts, *International Journal of Heat and Mass Transfer*, 133 (2019), Apr., pp. 1165-1175
- [30] Wang, Y., *et al.*, Characteristics of Heat Transfer for Tube Banks in Crossflow and Its Relation with that in Shell-and-Tube Heat Exchangers, *International Journal of Heat and Mass Transfer*, 93 (2016), Feb., pp. 584-594